EUROPHYSICS LETTERS 15 July 2001

Europhys. Lett., **55** (2), pp. 239–245 (2001)

Faceted drops on heterogeneous surfaces

T. Cubaud and M. Fermigier

Laboratoire PMMH, CNRS UMR 7636, ESPCI
10 rue Vauquelin, 75231, Paris Cedex 05, France

(received 14 August 2000; accepted in final form 3 May 2001)

PACS. 68.45.Gd – Solid-fluid interfaces: Wetting.

Abstract. – We report an experimental study of the shape of large liquid drops spreading on surfaces with patterns of wettability. A heterogeneous surface exhibits multiple energy minima of free energy for the three-phase system. In particular, when the distribution of defects on the substrate is periodic (square or hexagonal), it is possible to initiate a transition between circular and faceted drops. We describe the surface growth of these liquid drops as a geometric avalanche process released by surface tension.

Introduction. – The spreading of liquid films on solid surfaces is known to be strongly influenced by inhomogeneities and roughness of the solid. Recently, patterned surfaces with wettability contrast have been used to trap liquid droplets, in particular to create arrays of microreactors [1, 2]. Numerous microfluidic devices have been developed in particular for the analysis of biological molecules. Some of these devices rely on the existence of a wettability contrast on the substrate [3] and their successful operation requires the understanding of the anchoring of the moving contact line.

While the dynamics of wetting on a chemical homogeneous, smooth surface is well understood both at the macroscopic and microscopic levels [4, 5], wetting on heterogeneous surfaces still raises some questions. There are theoretical investigations of the distortion of a contact line due to wettability defects [6, 7]. The theoretical results are mostly limited to small contact angles and small deformations, because the general problem is difficult to solve analytically.

The deformation of the contact line due to a single defect was investigated in several experiments in a capillary-rise geometry [8–10]. In this case, the deformation is well described by existing analytical theories. The case of many defects was also investigated experimentally, again in a capillary-rise situation [11], in the imperfect Hele-shaw cell [12], for drops squeezed between solid surfaces [13] and more recently for liquid-He films [14].

This letter describes the occurrence of large sessile drops with faceted edges on substrates having wettability defects on periodic arrays, square or hexagonal. As a first step towards the understanding of collective pinning, we discuss the deformation of the contact line by isolated defects and the geometric parameters that drive depinning for a given defect, then we study the motion of the contact line in the case of a periodic distribution of line pinning centers and finally we show a shape transition of the drops as we change the defect strength.

Experimental set-up. – Heterogeneous substrates are prepared with a photolithographic technique described previously [12]. The substrates used in the experiments are silicon wafers (diameter 10 cm) with small circular islands (diameter in the range 100 μm–2 mm) of polymeric resin with a thickness on the order of 0.5 μm. The liquid used is a mixture composed of 60% of glycerol and 40% of water in volume. The capillary length for such a mixture is

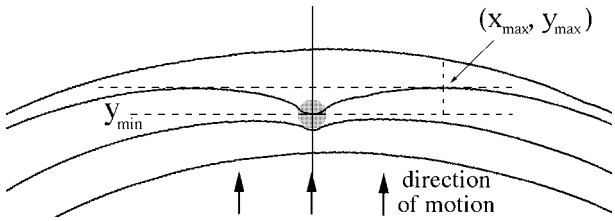

Fig. 1 – Pinning on a single defect (grey circle). Four subsequent positions of the contact line. The second line from the bottom shows anchoring on the defect edge. The third one shows motion over the defect.

2.44 mm ($\lambda_c = \sqrt{\gamma/\rho g}$, where γ is the surface tension of the liquid, ρ is the density of the liquid and g is the acceleration of gravity). There is a large difference of spreading coefficient for a glycerol/water mixture between the substrate itself and the thin layer of resin. Spreading of drops is studied, supplying a constant flow rate into the drop on substrates with various defect patterns. The drop evolution is followed from high-resolution (2032×2044) digital pictures taken from above. Using edge detection algorithms, the position of the contact line is determined at equally spaced times during the spreading. Contact line locations and defect positions, which are known precisely, are superimposed on composite images such as the one shown in fig. 7 below.

Isolated defects. – The typical diameter of the drops is much larger than the capillary length so that most of the drop-free surface is flattened by gravity. The three-dimensional deformation induced by the substrate is limited to the edge of the drop, but there are some large deformations of the contact line. The relevant parameter to describe the influence of a wettability defect is the dimensionless strength f which is defined as

$$f = \frac{\Delta S d}{\gamma h}, \tag{1}$$

where d is the defect diameter, h is the thickness of the drop, γ is the surface tension of the liquid and ΔS is the contrast in spreading coefficient between substrate and defect.

The defect strength can be understood as the ratio between the pinning force of the defect and the elastic restoring force due to surface tension. Experiments were performed varying the size of the defect d from 0.1 to 1.8 mm, corresponding to a range of dimensionless force f between 0.02 and 0.49. Figure 1 shows the deformation of the contact line on a single defect of diameter 0.6 mm. The contact line moves from bottom to top and the mean velocity of the line is 5 μm/s with a corresponding capillary number $Ca \approx 10^{-6}$. To quantify its deformation both in the direction of spreading and in the lateral direction of spreading, we plot the positions $y_{\min}$ and $y_{\max}$ of the two tangents to the contact line parallel to the mean direction of motion (see fig. 2). When the line is not distorted by the defect, we have $y_{\min} = y_{\max}$. We define the lateral extent of the deformation $x_{\max}$ as the x position where the line $y = y_{\max}$ is tangent to the contact line. The experiments show that $x_{\max}$ is a linear function of the defect size d. When $f < 0.4$, the curves $y_{\max}/d$ *vs.* $y_{\min}/d$ are superimposed showing that the contact line deformation in the direction of motion is a linear function of the defect size d. For higher values of f the deformation increases until $f \approx 0.6$, then the defect traps completely the contact line and prevents the coating of the defect by the liquid.

To characterize the shape of the contact line anchored on a defect, we define the pinning angle δ. It is defined as the angle between the two tangents to the contact line on each side

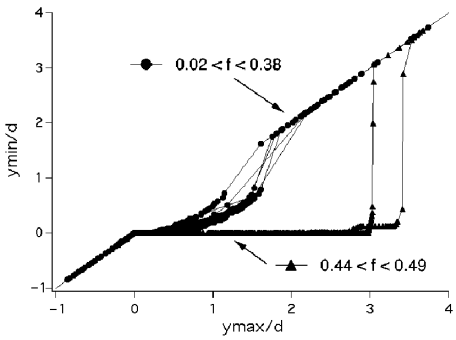

Fig. 2

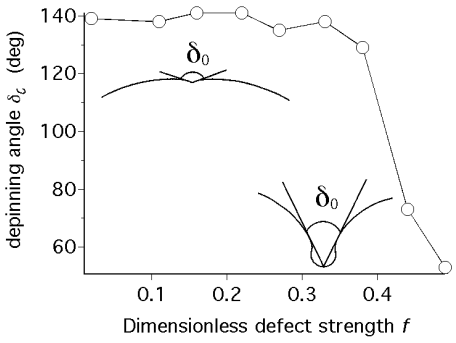

Fig. 3

Fig. 2 – Position of the bottom tangent to the contact line *vs.* position of the top tangent. Both positions normalized by defect diameters. The data for weak enough defects ($f < 0.4$) collapse on a single curve.

Fig. 3 – Depinning angle δ_0 *vs.* dimensionless defect force.

of the defect, whose intersection is the center of the contact line anchored to the defect. The pinning angle δ is equal to π in the early stage of the pinning process, then while the contact line deformation increases, δ decreases. Just before the triple line begins to advance on the defect, δ is minimal and equal to δ_0, the depinning angle. We have measured δ_0 for different defect strengths and, as can be seen in fig. 3, δ_0 remains constant for weak defects, with $f < 0.4$. This is consistent with the fact that both the amplitude of deformation $y_{\max} - y_{\min}$ and the lateral extent of deformation $x_{\max}$ scale with d.

Diluted defects. – Once we know the pinning behavior on a single defect, and particularly the depinning angle δ_0, we can find criteria for the contact line pinning on many defects, assuming that they are "diluted" enough. Since the drop is flat, the hydrostatic pressure is constant along the contact line. When the distance between defects is larger than $x_{\max}$, the shape of the drop edge is the same far from defects. The contact line is a set of circular arcs pinned on defects with a radius of curvature R. When the volume of liquid within the drops is increased, R decreases until the depinning angle δ_0 is reached on one of the pinning points. We can derive simple geometric relations using this assumption of constant radius of curvature. For an arc of line anchored on two defects, the angle β between the tangent to the contact line and the normal to the line passing through the center of the defects is such that $\cos\beta = \frac{L}{2R}$ (fig. 4, left), L being the distance between the defects. For two circular arcs anchored on three

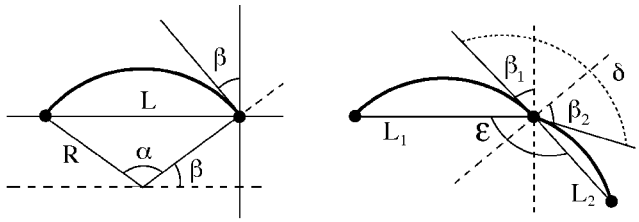

Fig. 4 – Simple anchoring model. Contact line anchored on two (left) and three (right) defects.

Fig. 5 – Large sessile drop on a hexagonal array of small non-wetting defects ($d = 0.4$ mm, $f = 0.08$, distance between defects = 0.707 mm), the width of the drop is 6 cm. The defect pattern and contact line motion for this drop are shown in fig. 8.

defects (fig. 4, right), the angle δ between the two arcs, on the central defect is

$$\delta = \arccos\left(\frac{L_1}{2R}\right) + \arccos\left(\frac{L_2}{2R}\right) + \pi - \epsilon\,, \tag{2}$$

where L_1 and L_2 are the distances between the defects and ϵ is the angle between the two lines joining the defects. For a given defect distribution, particularly for the periodic arrays considered in the following section, eq. (2) allows to predict where δ will reach the depinning angle δ_0 first.

Faceted drops. – In this section we discuss the case of a periodic distribution of line pinning centers. A periodic pattern (square or hexagonal) can be described with different rows of defect density. These rows represent energy barriers for the moving contact line, with a barrier height depending on the strength and the distance between defects. The rows with the maximum density (first and second neighbors) have the highest energy barriers. For the case of a square array of defects, there is a fourfold symmetry of the highest energy barriers and a sixfold symmetry for a hexagonal array. Surface tension acts in a way to minimize the free surface, so the wetted surface of the drop is as compact as possible. If the energy barriers of the rows are strong enough, they trap the edge of the drop. As a result of collective pinning, the shape of the wetted surface of a drop spreading on a square array of defects is a square according to the fourfold symmetry of the solid substrate. Likewise, on a hexagonal array, the shape of the wetted surface is a hexagon. An example of a drop spreading on a hexagonal array of defects is shown in fig. 5. As can be seen from this oblique view, the edges of the drop are straight and they form an almost perfect hexagon. On a periodic array, the distance and the orientation between defects in a row are the same, so the probability of depinning on each defect is the same. At a corner between two rows, the contact line remains anchored to the second neighbors. Using eq. (2), and its approximations, we have calculated the evolution of the pinning angle δ decreasing the radius of curvature R of the contact line for a defect on a row and for a defect at a corner (fig. 6). For a defect at a corner the distance to the next defect is larger than on a row but the angle ϵ is smaller than π. The calculation shows that for a square or a hexagonal array of defects, the depinning angle δ_0 is always reached first for a defect in a row than for a defect at a corner when $\delta_0 > 2\pi/3$. In our experiments on periodic patterns $f < 0.4$ and the observed value of δ_0 is 140 degrees. We expect then to see the depinning of the contact line first on the rows of defects.

In the present experiments, the liquid is injected at constant flow rate into the drop so the volume of liquid is continually increased. When the edge of the drop is completely trapped by the highest energy barriers, the thickness of the drop increases so the defect force decreases

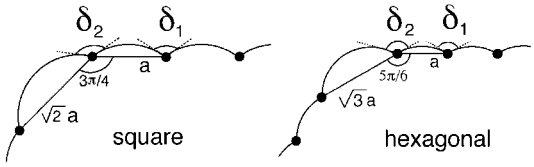

Fig. 6

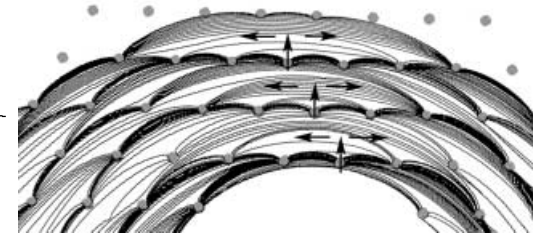

Fig. 7

Fig. 6 – Pinning angle δ at a corner of square and hexagonal arrays. All the circular arcs have the same curvature.

Fig. 7 – Subsequent positions of the contact line for a drop on a hexagonal array of defects ($d = 0.4$ mm, $f = 0.12$, distance between defects = 2.83 mm). The arrows show the contact line motion: depinning in the middle of a row of defects followed by motion along the row.

(eq. (1)). When defects are weak enough, the contact line start covering them, the increase of surface corresponds to the most compact surface growth. The facet on each row could be approximated as a straight line fixed at the corners of the 2D shape, so each line is an arc of circle which has an infinite radius of curvature. As the drop thickness increases, the hydrostatic pressure increases and the radius of curvature of the line decreases. This way, defects in the center of each row are covered the first. When they are totally covered the contact line relaxes, the depinning from one defect changes locally the pinning angles δ on the neighbor defects which depin up to them. The contact line is freed from these neighbor defects and fills a new row by an avalanche process. This depinning motion is shown in fig. 7 and fig. 8. The shape of the drops results from a dynamic growth process and not from a minimization of the global energy, because the contact line cannot explore different configurations through thermally excited motion. To investigate the stability of drop shapes, one should add energy fluctuations comparable to $\Delta S d^2$, for example, by vibrating the substrate [15]. In our case, for a given defect configuration, the faceted drops are stable. However, as explained in the following section, the occurrence of facets depends on the defect strength.

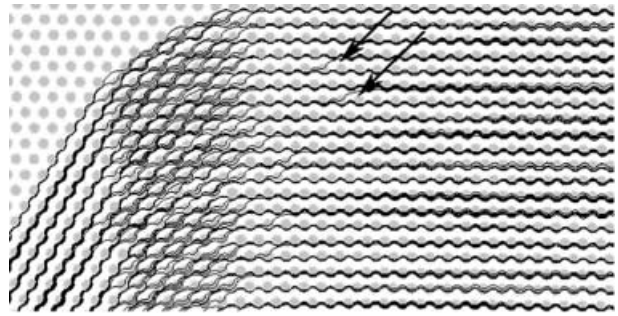

Fig. 8 – Motion of the drop edge on a hexagonal array of defects (grey circles). Top view of the drop shown in fig. 5. The arrows show a contact line moving sideways between two rows of defects ($d = 0.4$ mm, $f = 0.08$, distance between defects = 0.707 mm).

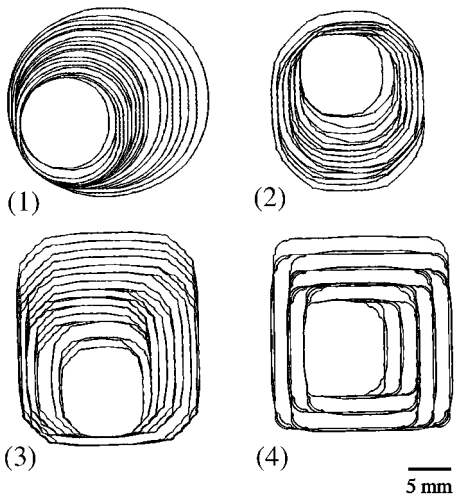

Fig. 9

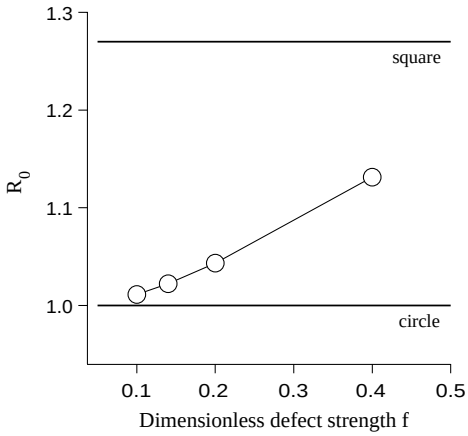

Fig. 10

Fig. 9 – Morphological evolution of a drop on different square patterns with different defect sizes: (1) $d = 0.5\,\text{mm}$, $f = 0.10$; (2) $d = 0.707\,\text{mm}$, $f = 0.14$; (3) $d = 1\,\text{mm}$, $f = 0.20$; (4) $d = 2\,\text{mm}$, $f = 0.40$.

Fig. 10 – Roundness parameter *vs.* defect force for the drops shown in fig. 9.

Shape transitions. – When the defect strength is small enough, we expect to observe drops with a circular edge on periodic defect arrays, because the minimization of the liquid-gas interfacial area will be prevalent over the minimization of the solid-liquid interfacial energy. We observed a shape transition from a circular drop to a faceted drop by increasing the defect size from 0.5 to 2 mm (f varying from 0.10 to 0.40) in a square array of defects (fig. 9). The shape of the defect is a square and the wettability contrast is inverse compared to the experiments described above (defects are wetting). The distance between defects is constant: $L = 0.352$ mm.

For small defect force, the macroscopic shape (the shape seen at length scales larger than the capillary length) of the drop is not affected by the solid surface topography. Increasing the defect force, the macroscopic shape changes from a circle to a square according to each square pattern. In order to quantify the shape transition, we define the mean "roundness" R_0 [16] of each shape as $R_0 = p^2/4\pi\Sigma$, where p is the drop perimeter and Σ the wetted surface.

R_0 is a function of the length scale at which the drop shape is examined. To determine R_0 shown in fig. 10, we choose the capillary length as a cut-off length, in order to remove the small-scale roughness of the contact line due to small defects ($d \leq 1$ mm). This small-scale roughness increases the perimeter of the drop and is not relevant to quantify the macroscopic shape. On the other hand, using this cut-off length removes the sharp corners of the square drop for $d = 2$ mm. As a result, the roundness parameter for drop (4) in fig. 9 is lower than 1.27, the value expected for a perfect square. The transition from a circle to a square is not a sudden jump, we observe intermediate octagonal shapes ((2) and (3) in fig. 9).

Conclusion. – The data obtained on the shape of the contact line anchored to a single defect suggests that, for small defects (dimensionless force less than 0.4), the maximum amplitude of deformation and the lateral extent of deformation are proportional to the defect size.

We have shown experimentally the existence of faceted liquid drops when macroscopic wettability defects are periodically ordered on plane substrate. In addition we have shown that there is a transition between circular and faceted drops when the defect force is varied. We interpret the existence of facets in terms of the local depinning force on the contact line which favors the growth along certain symmetry planes of the defect pattern. However, this phenomenon can also be understood as a competition between the meniscus elasticity and the anisotropy of the substrate surface energy. When the defect size (and the corresponding defect force) decreases, the meniscus elasticity eventually prevents the formation of facets. For this reason, the spreading of these large liquid drops has some similarities with crystal growth. The anisotropy of the substrate interfacial energy is here the analogous of the anisotropy of the surface tension between the crystal and the corresponding liquid. However, in our experiments, the influence of the thermal interface fluctuations is negligible because the energy involved in wetting a single defect is orders of magnitude larger than the thermal energy.

One of the questions which might be relevant to the operation of microfluidics devices and the positioning of drops on substrates is what is the lower limit (in terms of defect force) to get faceted drops? In other words, what are the minimum defect force and density which are able to maintain a straight drop edge against the meniscus elasticity? The data reported in fig. 10 suggest that below a dimensionless force $f = 0.1$, the anisotropy is too weak to create facets in the case of a non-wetting substrate with wetting defects. We are currently changing the technique to produce the defect patterns at much smaller scales to investigate this question.

* * *

We acknowledge financial support from Institut Français du Pétrole. The patterned substrates were prepared in Laboratoire de Microélectronique et Microstructures du CNRS with the help of D. Mailly. We also thank P. Jenffer for technical assistance, and L. Limat and J. M. Flesselles for fruitful discussions.

REFERENCES

[1] Jackman R. J., Duffy D. C., Ostuni E., Willmore N. D. and Whitesides G. M., *Anal. Chem.*, **70** (1998) 2280.
[2] Gau H., Herminghaus S., Lenz P. and Lipowsky R., *Science*, **283** (1999) 46.
[3] Burns M. A., Johnson B. N., Brahmasandra S. N. and Handique K., *Science*, **282** (1998) 484.
[4] Leger L. and Joanny J.-F., *Rep. Prog. Phys.*, **55** (1992) 431.
[5] de Gennes P.-G., *Rev. Mod. Phys.*, **57** (1985) 827.
[6] Joanny J. F. and de Gennes P. G., *J. Chem. Phys.*, **11** (1984) 552.
[7] di Meglio J.-M. and Shanahan M. E. R., *C. R. Acad. Sci. Paris*, **316** (1993) 1543.
[8] Cazabat A. M. and Heslot F., *Colloids Surf.*, **51** (1990) 309.
[9] Nadkarni G. D. and Garoff S., *Europhys. Lett.*, **20** (1992) 523.
[10] Marsh J. A. and Cazabat A. M., *Phys. Rev. Lett.*, **71** (1993) 2433.
[11] di Meglio J.-M., *Europhys. Lett.*, **17** (1992) 607.
[12] Paterson A. and Fermigier M., *Phys. Fluids*, **9** (1997) 2210.
[13] Chatain D. and de Jonghe V., *J. Adhesion*, **58** (1996) 163.
[14] Prevost A., Rolley E. and Guthmann C., *Phys. Rev. Lett.*, **83** (1999) 348.
[15] Andrieu C., Sykes C. and Brochard F., *Langmuir*, **10** (1994) 2077.
[16] Jain A. K., *Fundamentals of Digital Image Processing* (Prentice Hall) 1989, p. 392.